1. Chemical Evolution

1.1. Analytical Chemical Evolution Models

The data we hope to reproduce:

(1) the gas content of a stellar system as a function of time

(2) the overall metallicity in the gas as a function of time

(3) the metallicity distribution of the stars as a function of time

(4) the detailed abundances of various elements as a function of time in the gas

(5) the total mass of the system as a function of time

(6) the fraction of mass locked up in stellar remnants (neutron stars, white dwarfs) as a function of time

(7) the number of type of SN, neutron stars, novae, X-ray binaries, etc as a function of time

Observational data for most of these issues exists for the various components of the Milky Way galaxy, less detailed data exists for other nearby galaxies within the Local Group. Beyond the Local Group, the data is quite limited with regard to these issues.

1.2. Simple Homogenous Model

In a simple homogenous model, one assumes uniform mixing within the gas over the entire systmem, homogenous star formation, and no infall or outflow of gas from the system (i.e. a closed system). A power law initial mass function (IMF) $\phi(m)$ which is constant over time and space, is often assumed; the Salpeter value is $\phi(m)dm \propto m^{-2.35}\, dm$. More recent work by Scalo (1986, Fund.Cosmic Phys., 11, 1) and Kroupa (2001, MNRAS, 322, 231)

suggests that the Salpeter IMF is too steep to fit the observations for low mass stars below $0.5M_{\odot}$, and that a flatter slope is required, reaching -0.3 ± 0.7 for $0.01 < M/M_{\odot} < 0.08$. Note that the transformation from luminosity to mass (the IMF is a function of stellar mass) is not as well determined for the lowest mass stars). In their most recent work, Weidner, Kroupa & Bonell (2010, MNRAS, 401, 275) explore the statistical issues associated with massive stars forming in clusters. How does the maximum mass of a star formed in a cluster depend on the mass of the cluster gas ? Obviously a star with mass greater than this value cannot form in such a cluster. Integrating over many clusters with an appropriate cluster mass distribution, they then derive what they call the integrated galactic mass function, and which is somewhat steeper at the highest masses than a standard power law IMF.

Instanteous recycling, that stars die and release their metals very quickly after their birth, is also assumed. The specific simplifying assumption often made is that stars with $M < 1M_{\odot}$ live forever, while stars of higher mass die instantly. Since most metals come from fairly massive stars with lifetimes short compared to the age of the Galaxy, this is not an unreasonable assumption for an intial pedagogic model. Another assumption which must be made is that the fraction of mass from each stellar generation which remains locked up in long-lived remnants or in stars that do not evolve during the entire timescale of the calculation (i.e. the age of the Galaxy), α, is constant. This is equivalent to a constant IMF in practice.

In this case, following Francesca Matteucci (*The Chemical Evolution of the Galaxy*, Kluwer Academic Publishers, 2003) the equation for the metallicity as a function of time can be solved analytically. The variables are μ, the fraction of the total mass which is in gas that can form stars, p the nuclear reactions yield, and Z the fraction of metals in the gas (by mass). The subscript 0 denotes inital values when star formation first started in the system. M_s is the total mass in stars (both living and dead remnants) at the time t, M_g is

the fraction of the total mass in the form of gas at time t. $\psi(t)$ is the star formation rate, usually taken to be a function of σ_{gas}/τ_{dyn} (the Schmidt-Kennicutt law), where σ_{gas} is the surface density of gas and τ_{dyn} is the local dynamical timescale for collapse of a gas cloud. The current value of ψ in the local disk is $\sim 4 M_\odot pc^{-2}$/Gyr.

The relevant equations were first laid out by Beatrice Tinsley following earlier work by M. Schmidt (1959, 1963), and are given in many articles.

Conservation of mass and of heavy element abundance,

$$M_{gas} \; + \; M_s = M_{tot}, \quad M_s \; = \; (1 \; - \; \mu) M_{tot}, \quad Z \; = \; M_Z / M_{gas}.$$

The initial conditions are: $M_{gas}(t=0) \; = \; M_{tot}$ and $Z(t=0) \; = \; 0$.

The gas evolves according to

$$\frac{dM_{gas}}{dt} \; = \; -\psi(t) \; + \; E(t) \quad (eq.\ 1)$$

where $E(t)$ is the rate at which dying stars restore their gas to the ISM, partially enriched by nuclear reactions in their cores. $M_R(m)$ is the permanently locked up remnant mass for a star of mass m, and $\tau(m)$ is the lifetime of a star of mass m. Denoting $m(t)$ as the mass of a star born at $t = 0$ and dying at time t, we get:

$$E(t) \; = \; \int_{m(t)}^{\infty} (m - M_R) \psi(t - \tau_m) \phi(m) dm$$

The metallicity evolves through the addition of newly synthesized material from stars, namely:

$$\frac{d(ZM_{gas})}{dt} \;=\; M_{tot}\frac{d(Z\mu)}{dt} \;=\; -Z\psi(t) \;+\; E_Z(t) \quad (eq.\ 2)$$

where the second term represent the addition of material to the ISM from dying stars. This in turn has two components, the first is the pristine material from the outer layers of stars that was returned to the ISM without alteration, and the second is the processed material with newly formed and ejected metals, as indicated below in eq. 2a.

$$E_Z(t) \;=\; \int_{m(t)}^{\infty}[(m-M_R)Z(t-\tau_m) \;+\; mp_{Zm}]\psi(t-\tau_m)\phi(m)dm \quad (eq.\ 2a)$$

Define R as the total mass restored in pristine condition (i.e. without any products of nuclear reactions mixed in) to the ISM by each generation of stars. This is the gas lost by winds from the stellar surface. We assume that all stars with masses less than $1M_\odot$ always become remnants and never return any mass to the ISM; this defines the lower limit on the integral. Then R is:

$$R \;=\; \int_1^{\infty}(m-M_R)\psi(m)dm,$$

We also need the yield for nucleosynthesis, y_Z for the stellar generation, which is the ratio between the total mass of the isotope (element) i newly formed and ejected into the ISM from all stars with $M > 1M_\odot$, assumed to die immediately after being formed, and the amount of mass locked up in low mass stars and remnants,

$$y_Z \;=\; \frac{1}{1-R}\int_1^{\infty} m\; p_{Zm}\; \phi(m)dm,$$

where p_{Zm} is the mass fraction for a star of mass m of heavy elements freshly produced within the star and then ejected into the ISM upon its death. We denote the yield y_Z as

the effective yield $y_{Z_{eff}}$ which describes the stellar system assuming that the Simple Model is adequate. If $y_{Z_{eff}} > y_Z$ then the system has attained a higher metallicity for a given gas fraction μ than the Simple Model can produce. If this were the case, then some assumption in the Simple Model must be incorrect.

Substituting eq. 2 into eq. 1 and assuming instantaneous recycling, which allows us to neglect τ_m, we end up with an equation

$$E_Z(t) = \psi(t)RZ(t) + y_Z(1-R)\psi(t).$$

This simplifies, in the Simple Model, to

$$\mu\frac{dZ}{dt} = -y\frac{d\mu}{dt}$$

which has the solution

$$Z = y_Z\, ln(1/\mu). \quad (eq.\ 3)$$

This is the fundamental equation for the evolution of metallicity with time in the Simple Model. Z is a function of the fraction of the total mass that is in the form of gas that can be used to form stars, μ. Once a value is assigned to μ, Z can be calculated, assuming the nuclear yield per generation of stars, y, is known.

1.3. Applications of the Simple Model

We can now calculate the fraction of all stars ever formed with metallicities less than or equal to Z, $S(Z)$. We first calculate the fraction of all stars formed while the gas fraction

was $\geq \mu$, $(M_*/M_1) = (1-\mu)/(1-\mu_1)$, where the subscript 1 denotes the present value. All these stars were formed with $Z < y_z\ ln(1/\mu)$. So the fraction of stars today with metallicities $\leq Z$, indicated by $S(Z)$ is

$$S(Z) \ = \ \frac{1 - exp(Z/y_Z)}{1-\mu_1} \ = \ \frac{1-\mu_1^{Z/Z_1}}{1-\mu_1}. \quad (eq.\ 4)$$

The average stellar metallicity can be calculated as well. This will be a mass-averaged metallicity, unless a specific mass-luminosity relation is put in to the integral as well to give a luminosity averaged metallicity. Since the luminosity is dominated more by giants than is the mass, the two may be different, and in general the luminosity weighted metallicity is smaller than the mass-averaged one.

If we find the gas fraction μ at which half of the stars observed today have formed, we can find the associated Z, which will be the median of the metallicity distribution. Assuming μ at the present time in the Solar neighborhood is ~ 0.5, we get $Z(median) \ = \ 0.3\ y_Z$. Thus since in the Solar neighborhood the mean Z is about 0.5 that of the Sun, we infer that the present value of y_Z is $\sim 1.7\ Z_\odot$.

A comparison of the predictions of the Simple Model with the Solar neighborhood metallicity distribution, $S(Z)$, shows that there are fewer metal-poor stars predicted by the Simple Model than are observed. This is often called the "G dwarf problem".

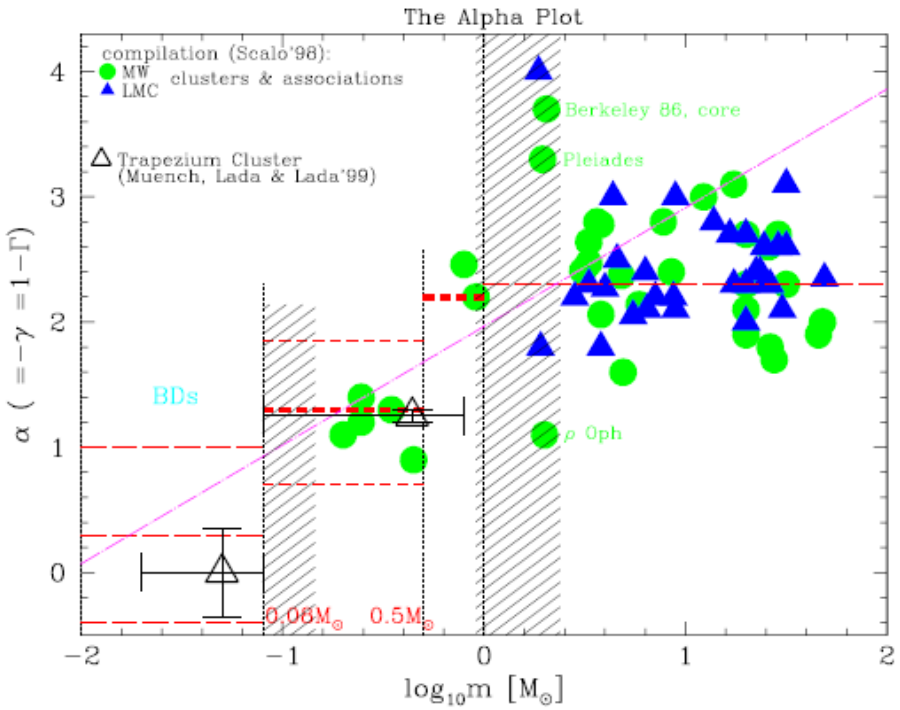

Figure 1. The *alpha-plot* for Milky-Way (MW) and Large-Magellanic-Cloud (LMC) star-clusters and associations. Data are from the compilation of Scalo (1998). The horizontal dashed lines are the average IMF with estimated uncertainties (eqn 2), and the diagonal dot-dashed line is the popular Miller-Scalo (1979) IMF. From Kroupa (2001b). The figure can be obtained in colour from astro-ph/0009005.

Fig. 1.— The IMF slope inferred from various Milky Way and LMC clusters (from Kroupa, 2001, MNRAS, 322, 231). The horizontal line in the right half of the figure is the Salpeter slope, which appears to fit the IMF for stars more massive than $1M_{\odot}$.

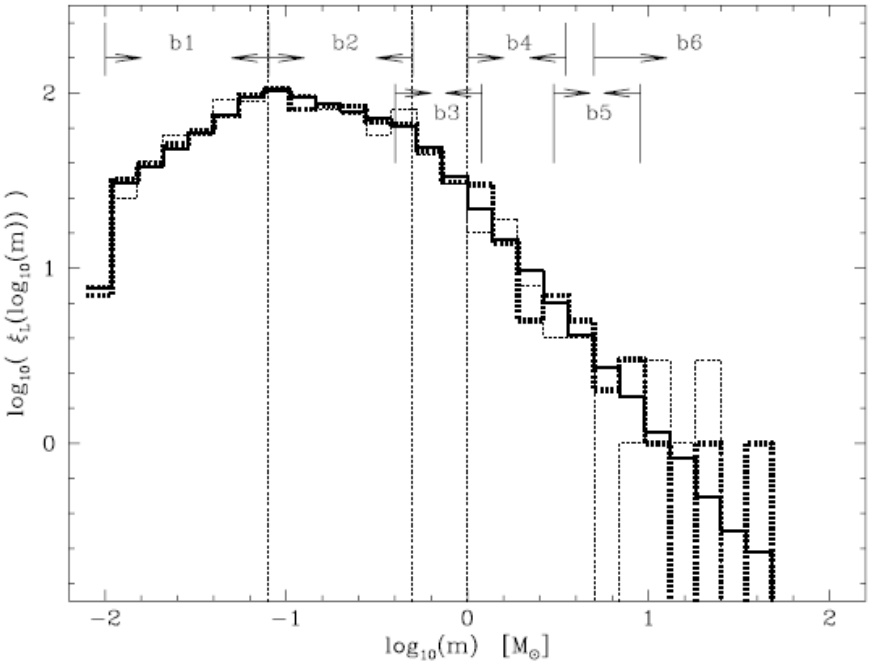

Fig. 2.— The adopted logarithmic IMF (eqs. 2 and 3), $\xi_L/10^3$, for 10^6 stars (solid histogram). Two random renditions of this IMF with 10^3 stars are shown as the heavy and thin dotted histograms. The mass-ranges over which power-law functions are fitted are indicated by the arrowed six regions (eq. 4), while thin vertical dotted lines indicate the masses at which α_i changes.

Fig. 2.— from Kroupa (2001, MNRAS, 322, 231)

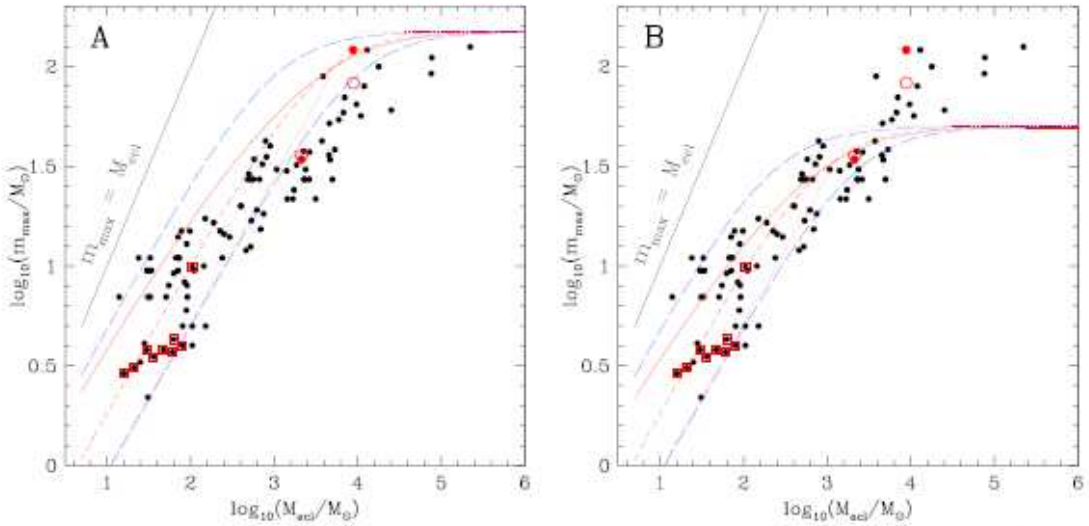

Figure 5. *Panel A*: Most-massive star vs cluster mass. The dots are the observed values from column # 4 from Tab. B1. The two *open circles* indicate existing dynamical estimates for the present-day mass of the most-massive stars. The *boxed* data are from the sample of Faustini et al. (2009). The *dotted* line refers to the mode value for random sampling, the *short-dashed* line to the median value, the curved *solid* line marks the mean value and the two *long-dashed* lines are the 1/6th (lower) and 5/6th (upper) quantiles between which 2/3rd of the data points should lie if they were randomly sampled from the IMF over the mass range 0.01 $M_\odot$ to $m_{max*} = 150\ M_\odot$. The thin *solid* line to the left marks the identity where the cluster is made-up only of one star. *Panel B*: The same as *panel A* but assuming a fundamental upper mass limit for stars of $m_{max*} = 50\ M_\odot$ instead of 150 $M_\odot$.

Fig. 3.— The mass of the highest mass star known in each of a set of young clusters as a function of the total mass of the cluster. from Weidner, Kroupa & Bonnell 2010)

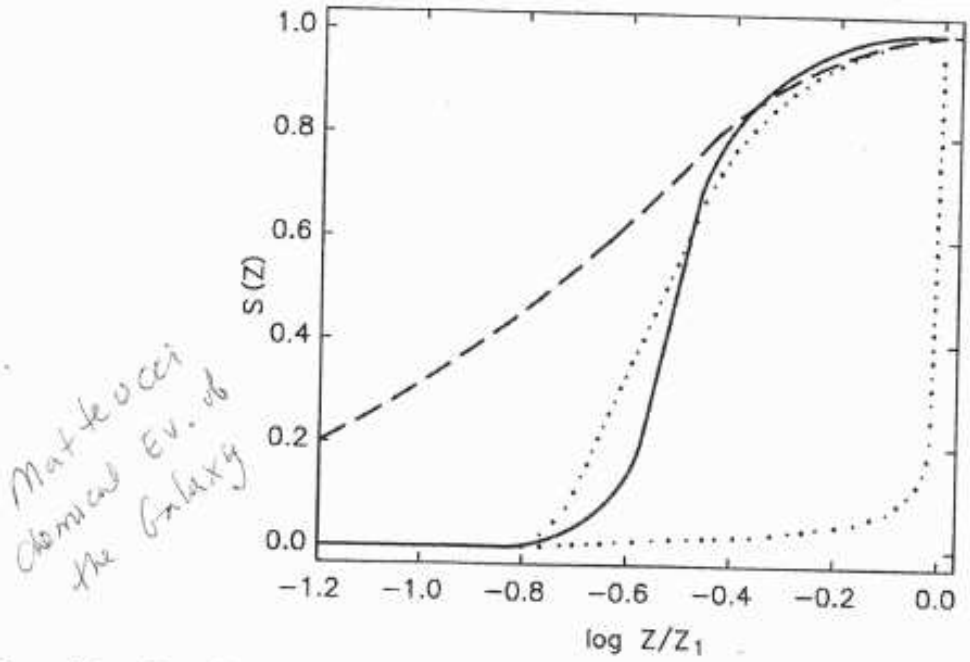

Figure 5.1. Cumulative stellar metallicity distribution. S(Z) is the fraction of stars having metallicities $\leq Z$, with a maximum value Z_1 (taken as $2Z_\odot$). *Solid line*: log-normal representation of the data for the solar neighbourhood. *Long dashes*: the prediction of the Simple Model for the chemical evolution. *Short dashes*: the prediction of the extreme infall model. *Dots*: prediction of a model with a finite initial metallicity. From Tinsley 1980, Fund. Cosmic Phys. Vol. 5, 287; reproduced here by kind permission of Gordon & Breach Science Publishers (copy right 1980).

Fig. 4.— Fig. 5.1 of Matteucci's book *The Chemical Evolution of the Galaxy.*

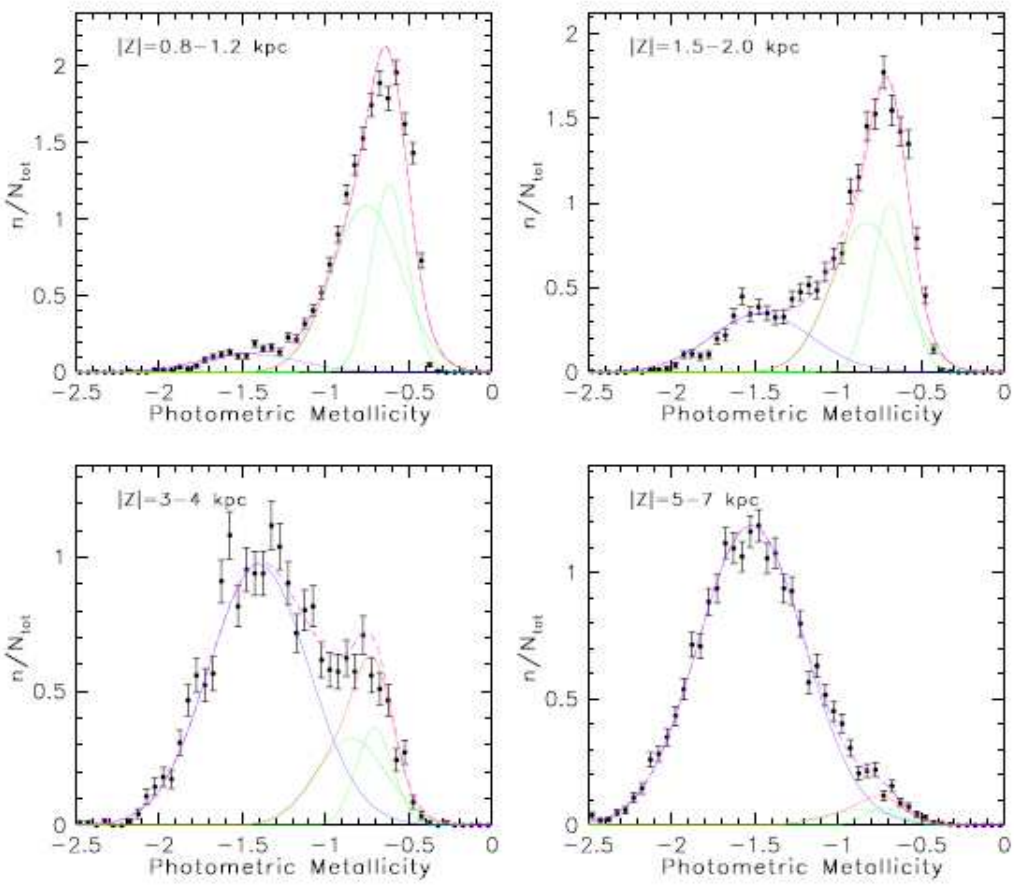

FIG. 7.— The symbols with error bars show the measured photometric metallicity distribution for stars with $0.2 < g - r < 0.4$, 7 kpc $< R <$ 9 kpc, and distance from the Galactic plane in the range 0.8–1.2 kpc (top left, ∼6,200 stars), 1.5–2.0 kpc (top right, ∼3,800 stars), 3.0–4.0 kpc (bottom left, ∼2,800 stars) and 5.0–7.0 kpc (bottom right, ∼6,000 stars). The histograms are essentially horizontal (parallel to x axis) slices at corresponding $|Z|$ intervals through the map shown in the top right panel of Figure 5. The dashed magenta lines show a best-fit two-component, halo plus disk, model. The blue lines show the halo contribution, modeled as a single Gaussian, and the red lines show the contribution of a non-Gaussian disk model, modeled as a sum of two Gaussians shown by the green lines. See § 3.3.1 and Table 3 for the best-fit parameters.

Fig. 5.— The metallicity distribution of the thick disk in the Solar neighborhood, and in the halo, from Ivezic et al (SDSS), 2008, ApJ, 684, 287

1.4. Secondary Elements

An element is secondary if it is produced in reactions proportional to the initial metallicity of the star, not just from hydrogen and He. The heavy elements beyond Fe, for example, are produced by neutron capture by the pre-existing Fe nuclei. Until some Fe exists, they can't be produced.

In this case, eq. 2 becomes:

$$E_s \;=\; \int_{m(t)}^{\infty} [(m - M_R)\; X_S\; (t - \tau_m) \;+\; m p_{sm}\; \frac{Z(t-\tau_m)}{Z_\odot}] \psi(t-\tau_m) \phi(m) dm. \quad (eq.\ 5)$$

Under the assumption of instantaneous recycling, this eventually becomes $X_S \propto Z^2$ $(eq.\ 6)$ in the Simple Model.

1.5. Other Analytical Cases

Analytical solutions exist for a number of other cases. If one wishes to add accretion of gas as well as Galactic outflows, then the total mass of the system may change with time.

$$\frac{dM_{tot}}{dt} \;=\; -\,W(t) \;+\; A(t) \quad (eq.\ 7)$$

where $W(t)$ represents the Galactic wind (outflow) and $A(t)$ the accreted material, assumed to have metallicity Z_A.

The equation for the evolution of the metallicity is then:

$$\frac{d(Z\; M_{gas})}{dt} \;=\; -\,Z(t)\; \psi(t) \;+\; E_Z(t) \;+\; Z_A(t) A(t) \;-\; Z(w) W(t) \quad (eq.\ 8),$$

where the last two terms on the right side represent accretion and outflow, while the first two terms represent removing material from the ISM via star formation and adding processed material back to the ISM upon stellar death.

Analytical solutions exist in certain specific cases. First, if one ignores accretion and defines the wind term as proportional to the star formation rate, $W(t) = \lambda(1 - R)\psi(t)$, where λ ($\lambda \geq 0$) is the wind parameter, the solution is:

$$Z \;=\; \frac{y_Z}{1+\lambda} ln[(1+\lambda)\mu^{-1} \;-\; \lambda] \quad (eq.\ 9)$$

The true yield is always lower than the effective yield for outflows.

If one has accretion without any outflow, and the accretion rate is set to $A(t) \;=\; \Lambda(1 - R)\psi(t)$, where $\Lambda > 0$ is the accretion parameter, and where the infalling gas has $Z_A \;=\; 0$, then the solution for $\Lambda \neq 1$ is:

$$Z \;=\; \frac{y_Z}{\Lambda}[1 - (\Lambda - (\Lambda - 1)\mu^{-1})^{-\Lambda/(1-\Lambda)}] \quad (eq.\ 10a)$$

and for $\Lambda = 1$ is

$$Z \;=\; y_Z[1 - e^{-(\mu^{-1}-1)}] \quad (eq.\ 10b).$$

The latter is the solution for extreme infall where the amount of gas remains constant in time, that going into stars is replaced by infalling primordial gas. In this case, $(\mu^{-1} - 1)$ is the ratio of the accreted mass to the initial mass.

A somewhat more complicated expression can be derived for the analytical solution for both accretion and outflows being present provided that $A(t)$ and $W(t)$ can be represented

as parameterized above. See eqtn. 5.43 of Matteucci, *The Chemical Evolution of the Galaxy.*

Clayton (1985, 1987, see 1987, ApJ, 315, 451) described another family of cases which are exactly soluble. His cases allow more freedom in parameterizing the star formation rate and the infall rate. He begins by assuming that the star formation rate is a linear function of the gas mass, $(1 - R)\psi(t) = \omega M_{gas}$, where ω is a constant. Exact solutions exist to this model if $A(t)$ has the form

$$A(t) \;=\; \frac{k}{t + \Delta} M_{gas}(t),$$

where k and Δ are free parameters.

The Clayton model is useful as one can study analytically a wider range of SF histories and infall rates than can be done in the simpler models described above.

A variation of Clayton's model developed by Pagel (1989) introduces a fixed delay between the star formation and the stellar death, which allows one to study the behavior with time of elements such as Fe which are formed on long timescales. For a linear star formation rate and a fixed time delay Δ and for a wind parameter λ he found the analytical solution:

$$Z(t) \;=\; y_z \; e^{(1+\Lambda)\omega\Delta} \; \omega(t - \Delta).$$

At present these analytical models are used as pedgogical tools and for testing numerical codes only.

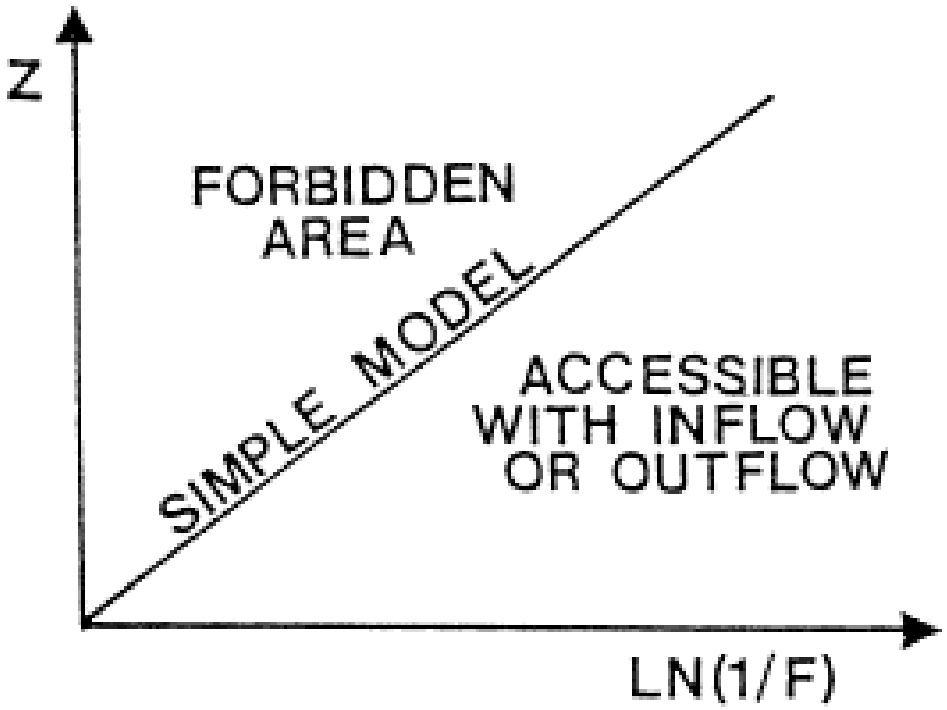

Figure 1. Schematic plot of metallicity z versus logarithm of the reciprocal of the gas fraction $\ln(1/f)$ for galaxies, or regions of galaxies, to show the area of the plot which can be reached by inflow of *unenriched* gas or outflow.

Fig. 6.— Fig. 1 of Edmnds, 1990, MNRAS, 246, 678. Note that F in his notation is $\mu = M_{gas}/Mtot$ in the notation used here.

1.6. Timescale for Chemical Evolution

We assume the simple model with instantaneous recycling. The star formation timescale = time to consume all the gas in a system,

$$\tau_* \;=\; \frac{M_{gas}}{abs[dM_{gas}/dt]} \;=\; \frac{M_{gas}}{(1-R)\psi},$$

which evaluated for the solar neighborhood yields $\tau_* \sim 1$ Gyr. This seems too short, another symptom that the Simple Model is too simple for the solar neighborhood.

The timescale for chemical enrichment, τ_Z, necessary to reach the metallicity Z is

$$\tau_Z \;=\; \frac{Z}{abs[dZ/dt]} \;=\; \frac{ZM_{gas}}{abs[y_Z(1-R)\psi]} \;=\; \tau_*(Z/y_Z)$$

This is about 1 Gyr, which is too short a timescale. We need infall to fix up the problems the simple model encounters when applied to the Solar neighborhood.

2. Numerical Computations of Chemical Evolution

The equations to be solved are the equivalents of eq. 1 and eq. 2 with the additional terms appropriate to the situation being considered. The star formation rate may vary with time; it is usually taken as exponentially declining with time with a timescale τ_0 set to best fit the data for the situation under consideration, $\phi(t) \;=\; Aexp(-t/\tau_o)$. The value of τ_0 is set short to match old stellar populations (elliptical galaxies), perhaps ∼1 Gyr, and longer to replicate spiral galaxies (∼5 Gyr), and even longer to model dwarf irregular galaxies

There may be infall and/or outflows. There may be radial mixing or other forms of spatial non-uniformity. You may want to abandon the instantaneous recycling

approximation, using $f(t-\tau_m)$ instead of the simpler $f(t)$. After all, once you go for a numerical solution, it might as well be as good as you can make it.

The key equation for each element (isotope) i considered has the form:

$$\frac{dG_i}{dt} \;=\; -\,\psi(t)X_i(t) \;+\; X_{iA}(t)A(t) \;-\; X_i(t)W(t) \;+\; \text{many source terms.}$$

Each of the source terms is similar to:

$$\int_{M_L}^{M_u} \psi(t-\tau_m)Q_{mi}(t-\tau_m)\phi(m)dm.$$

Here $X_i(t)$ is the fractional abundance by mass of the species i, $G_i(t) = \sigma_i/\sigma(t_G)$, where σ is the total surface mass density, including gas and stars, both living and dead. The first three terms on the right include gas lost from the ISM due to star formation, accretion of material which has an abundance of species i of X_{iA}, and outflows. Then follow a number of source terms which are of the general form shown above, namely an integral over a range of stellar mass times a production rate $Q_i(t)$ and the initial mass function. These can be from various types of supernovae, novae, AGB stars, or any other source.

There is another equation which gives the total gas mass including accretion and outflows.

The exact form of these equations will depend on the specific problem to be solved, the galaxy to be modelled, etc. The basic equations are not hard to write down, and in such circumstances can best be solved numerically. If you want to follow the abundances of various elements besides H in detail, you will need a full set of nucleosynthetic yields and, in particular for non-primary elements/isotopes, there may be a lot of coupling between the equations for the various elements to be included. Overall, however, this is a trivial

calculation on the scale of current computing capabilities, easily carried out on a personal workstation.

3. Rates of SNIa, SNII, Novae, AGB Stars, PISN

SN rates can be predicted from the IMF and star formation rate. We also now have good observational data from very large imaging surveys attempting to detect SN of actual rates in various galaxies. Such surveys include the Supernova Legacy Survey (SNLS) carried out at the CFHT, the Palomar Transient Facility now in operation, etc. Wide field imaging at high cadence is required for this purpose. We first describe the predicted rates, then the observations. Because of the high absorption in the Galactic plane and the fact that these stellar explosions are rare, it is quite difficult to determine these rates from the Milky Way.

3.1. Rates from Models

The SNII rate is easy to calculate. It has two terms, the first from those stars in the mass range such that if they were in a binary system, they do *not* become SNIa. The parameter A represents the fraction in the IMF of binary systems with the right properties to become SNIa. The second term includes stars more massive than that that up to the highest mass present, M_{up}, usually between 40 and $100M + \odot$. The first integral goes from $M1$, the lowest mass for which a degenerate CO white dwarf can form, to $M2$, the highest mass for this can occur taking into account mass loss. Values from 6 to $8M_{\odot}$ are often used for $M2$. The second integral runs from $M2$ to the highest mass star in the system M_{UP}. The parameter A is the fraction in binaries which become SNIa.

$$R(SNII) \; = \; (1-A)\int_{M1}^{M2}\phi(M)\psi(t-\tau_m)dM \; + \; \int_{M2}^{M_{UP}}\phi(M)\psi(t-\tau_m)dM$$

SNII rates should be strictly proportional to the very recent star formation rate $SFR(t)$ in a galaxy. Since star formation increases at higher redshift by a factor of about $(1+z)^{3.5}$,

one expects the SNII rate to increase by this factor as well.

Greggio (2010, MNRAS, in press, see arXiv:1001.3033) gives rates for SNIa. Thes are believed to originate from degenerate binaries, both singly degenerate and systems where both components are degenerate (doubly degenerate). A detailed understanding of binary star frequency and evolution, including, for example, decay of the binary orbit due to loss of energy by gravitational waves, is required to evaluate the rate properly. In order to produce a SNIa, the binary must be a close binary, the primary of the binary must be an intermediate mass star (2 to 8 $M_{\odot}$) so the first Roche lobe overflow leading to mass transfer to the secondary must leave a CO WD, i.e. the core of the primary star.

She calculates the delay time between the initial formation of the stars and the SNIa explosion. This is the crucial delay between SNIa and SNII (core-collapse SN, which for massive stars occurs almost instantaneously as their lifetimes as so short).

Novae are similar to SNIa, in that they too involve degenerate white dwarfs in a binary system, with mass transfer. But a nova explosion involves only the accreted material. The explosion is less energetic and the net effect is the loss of some material, but the white dwarf itself is not disrupted. Nova rates were calculated for a constant SFR model by Yungelson, Livio & Tutukov (1997, ApJ, 481, 127). The nova rate is proportional to the rate of formation of white dwarfs. But they must be in the appropriate binary systems in order to have novae occur. Many details of the evolution of binary systems are required to carry out this calculation.

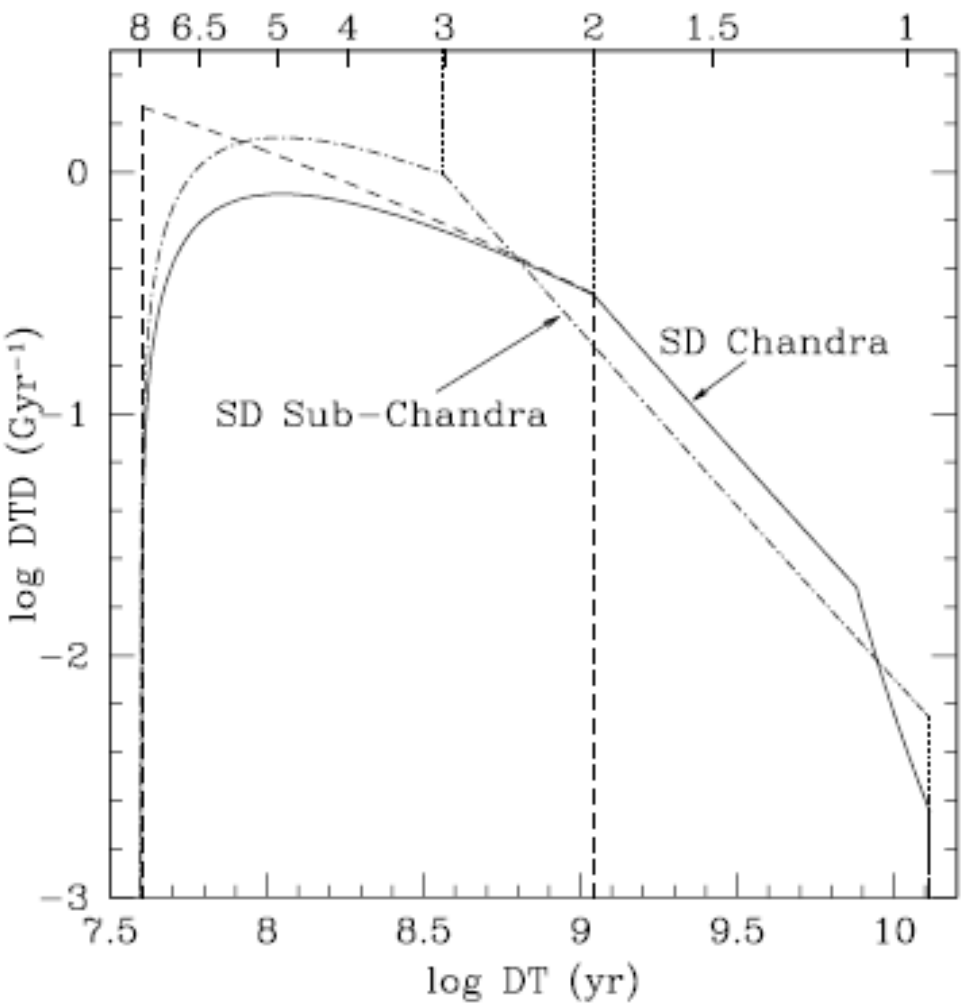

Figure 1. Distribution of the delay times for SD models, Chandra (solid) and Sub-Chandra (dot-dashed). The DTD is normalised to 1 over the range 0.04 to 13 Gyr. The upper axis is labelled with the value of the stellar mass (in $M_\odot$) evolving off the MS at the corresponding a delay time labelled on the lower axis. A Salpeter IMF for the primaries, a flat distribution of the mass ratios, and $m_1 \geqslant 2$ (3) $M_\odot$ for Chandra (Sub-Chandra) models have been adopted. The dashed line shows the trend of the CO WD formation rate from the primaries, which may represent an upper limit to the slope of the DTD for the MS+WD channel. This function, plotted on the logarithmic scale, is not normalised to 1 over the delay time range.

Fig. 7.— SD = singly degenerate, i.a. a binary in which only one component is a white dwarf. Fig. 1 of Greggio (2010).

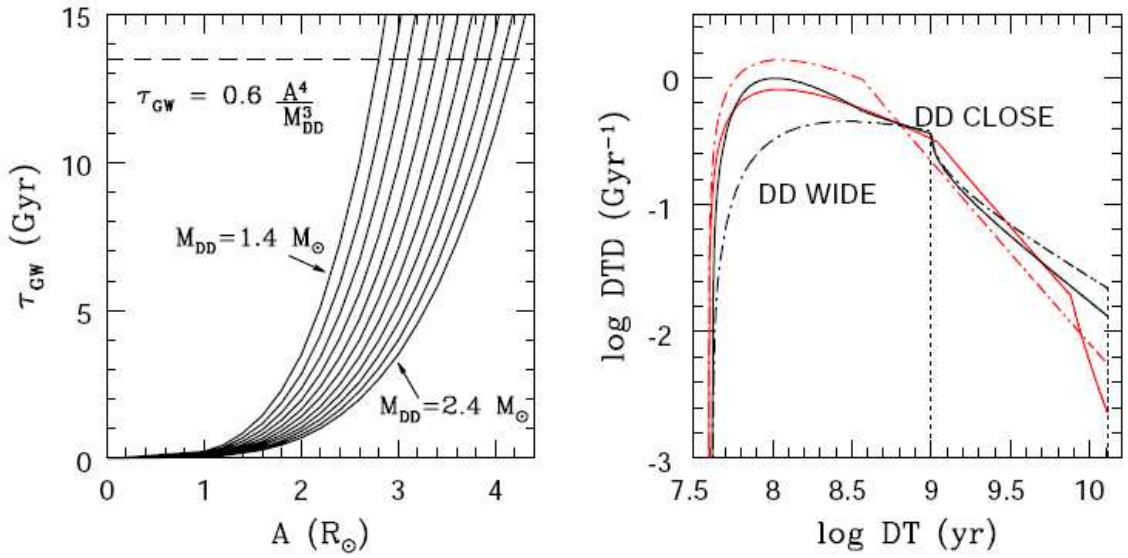

Figure 2. Left: the delay time due to the gravitational wave radiation, as given by the labelled (approximate) relation, as function of the initial separation of the DD systems, and for M_{DD} ranging from 1.4 to 2.4 $M_\odot$ in steps of 0.1 $M_\odot$. Right: the distribution of the delay times for DD models, CLOSE (solid) and WIDE (dot-dashed), in the same units as in Fig. 1. Adopted parameters include a Salpeter IMF for the primaries, a flat distribution of the mass ratios, $\tau_n \leqslant 1$ Gyr, and flat distribution of the separations A. The DTDs for the SD models are plotted in red for comparison.

Fig. 8.— DD = doubly degenerate, a binary with both components being degenerate white dwarfs. Fig. 2 of Greggio (2010).

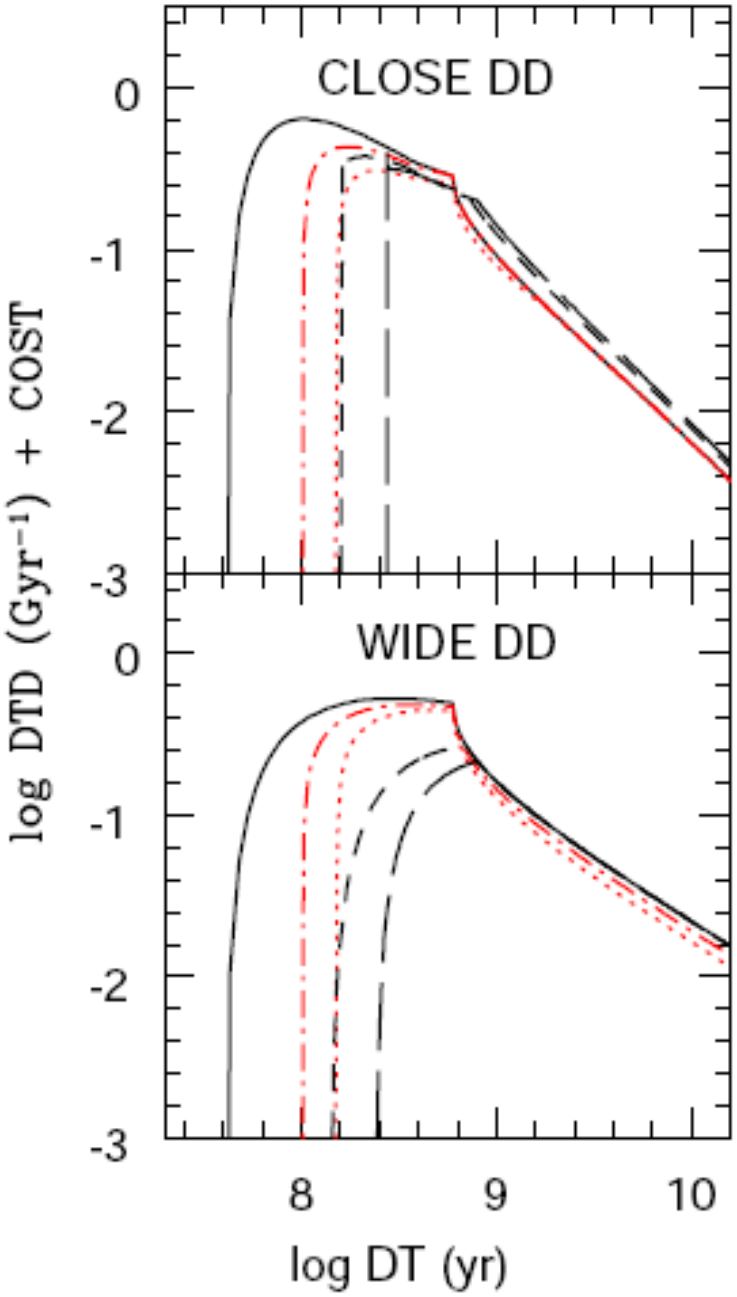

Figure 7. Effect of varying the minimum evolutionary lifetime ($\tau_{n,0}$) and gravitational wave radiation delay ($\tau_{CW,0}$) in SN Ia progenitor systems for DD CLOSE (top) and WIDE (bottom) models. The line-types encodes the values of ($\tau_{n,0}$,$\tau_{CW,0}$) = (0.04,0.001) (solid), (0.1,0.001) (dot-dashed, red), (0.15,0.001) (dotted,red), (0.04,0.1) (short dashed), (0.04,0.2) (long dashed). All curves assume a minimum m_2 of 2.5 $M_\odot$, and a flat distribution of A.

Fig. 9.— Fig. 7 of Greggio (2010).

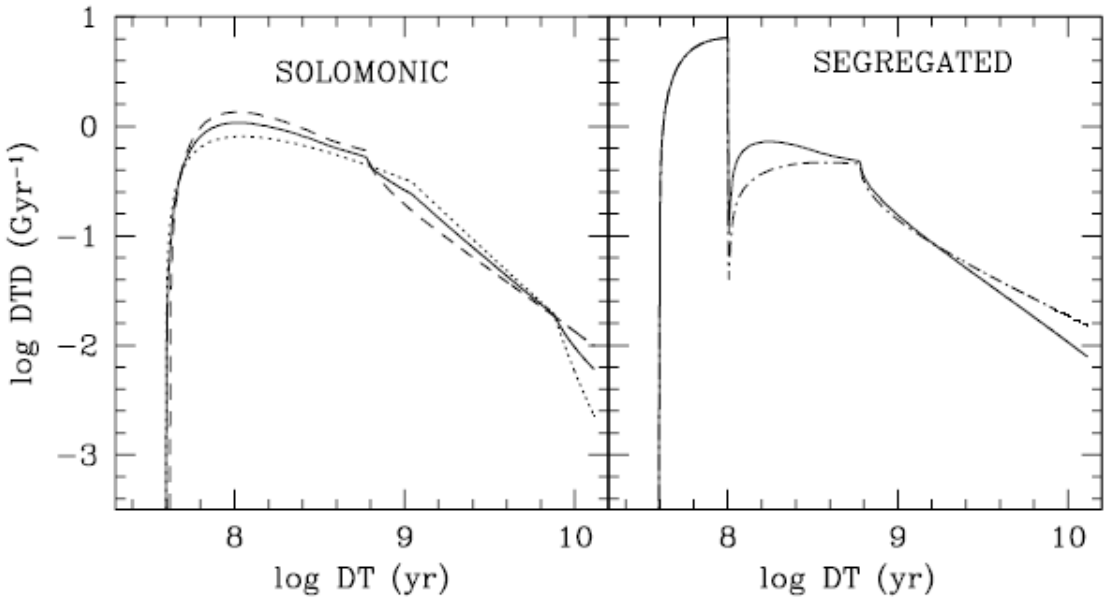

Figure 9. DTDs for mixed models. Left: the DTD of SD Chandra explosions in Fig. 1 (dotted line) is combined with the DTD of a DD-CLOSE model with minimum secondary mass of 2.5 $M_\odot$ and a flat distribution of A (dashed) to construct the Solomonic mixture, in which 50 % of the total events within 13 Gyr come from either channel. Right: the events at delay times shorter than 0.1 Gyr come from SD explosions, while those at longer delay times come from the DD-CLOSE (solid) or DD-WIDE (dot-dashed) evolutionary channels, both with minimum m_2 of 2.5 $M_\odot$ and a flat distribution of A. The events from the SD channel amount to 30 % of the total within 13 Gyr.

Fig. 10.— Solomonic model: SD and DD each contribute half of the total events at all times. Segregated model: SD explosions provide early events, DD provide longer delay time events. (Fig. 9 of Greggio 2010).

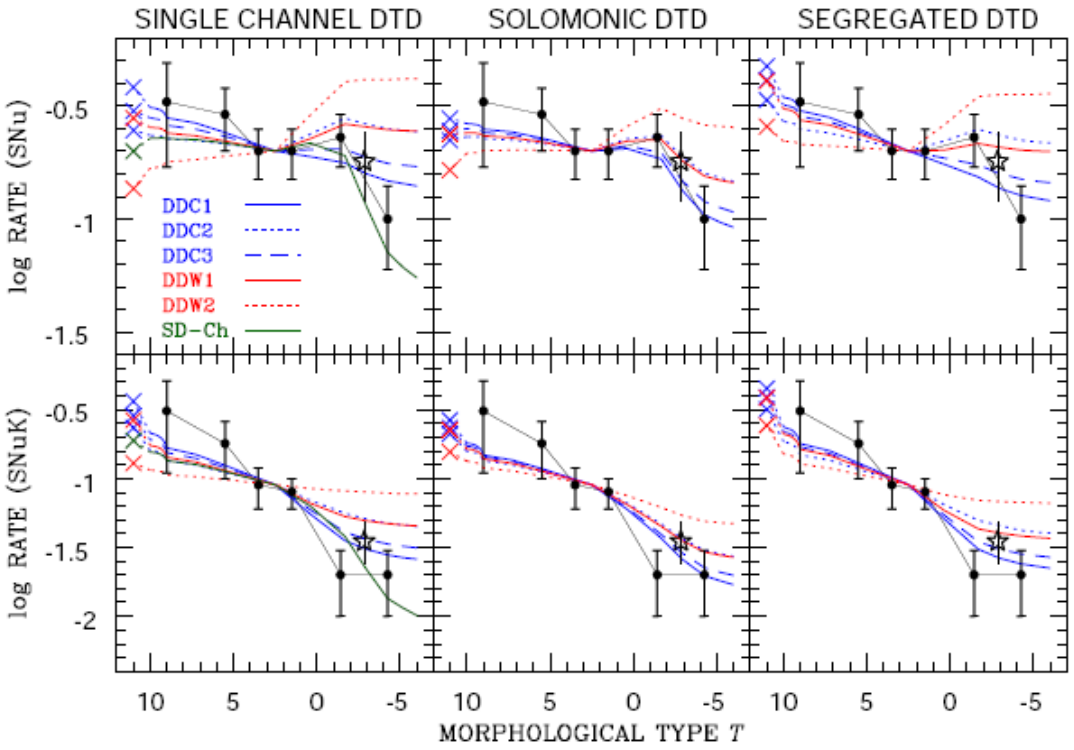

Figure 11. SN Ia rate per unit B (upper panels) and per unit K (lower panels) luminosity, as function of the morphological type of the parent galaxy. Black dots show the observed rates from Greggio & Cappellaro (2009); the stars shows the published rates for the E+S0 class; coloured lines show models calculated with different DTDs and the SF rate given by Eq. (5). Left panels: theoretical relations obtained with single channel DTDs. The SD Chandra (SD-Ch.m green line) model assumes a Salpeter distribution for m_1, a flat distribution of the mass ratios, and an efficiency $\epsilon = 1$. Blue lines are obtained with DD-CLOSE models; DDC1 and DDC3 assume a distribution of separations skewed at small values, and differ for the minimum m_2, respectively of 2.5 and 2 $M_\odot$; DDC2 assumes a flat distribution of the separations and a minimum m_2 of 2.5 $M_\odot$. Red lines are obtained with DD-WIDE models, DDW1 and DDW2 being computed with the same choice of parameters as DDC1 and DDC2. Central and right panels: correlations obtained with mixed DTDs in the Solomonic and Segregated flavours; colours and line types reflect the specific DD model used to construct the mixture with the encoding labelled in the top left panel. The coloured crosses show the rates for the bursting model in Fig. 10 put at an arbitrary value of T.

Fig. 11.— DTD = delay time distribution. The X axis of this plot roughly indicates the galaxy type, 10 being extreme spirals and irregulars with high star formation rates, −5 being ellipticals with no current star formation. (Fig. 11 of Greggio 2010).

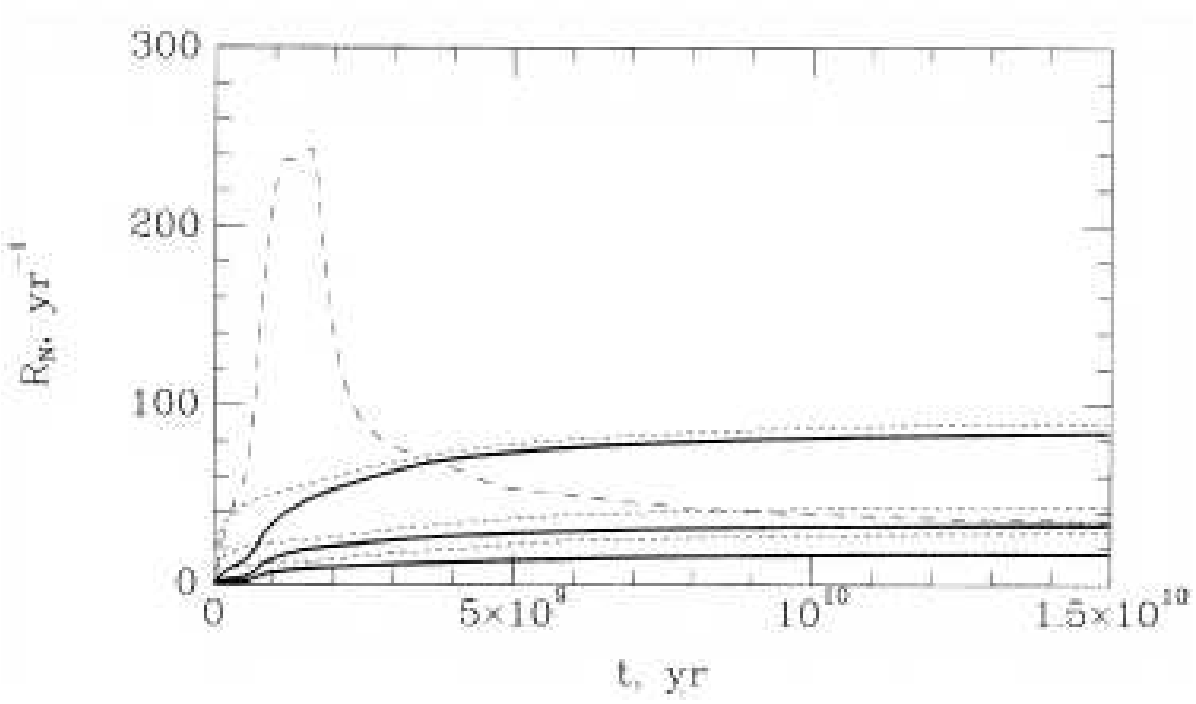

Fig. 12.— Fig. 1 of Yungelson, Livio & Tutokov (1997). Pairs of curves correspond to different distributions of binaries over the mass ratios of the components $f(q) \propto q^{\alpha}$, for $\alpha = -1, 0, 1$ from top to bottom. The two lines for each of the three values of α modeled correspond to different parameters for the common-envelope phase. The long dashed line describes the nova rate for a 10^9 yr initial burst of star formation followed by a stage of constant (lower) star formation for another 14 Gyr so that equal total stellar masses were formed in the burst and in the extended constant SFR phase. The total mass in each case is $15 \times 10^9 M_{\odot}$, close to that of the Milky Way, so th is is a prediction of the nova rate for our galaxy.

3.2. Observed SN Rates

SNIa have been the subject of intensive study because of their use as cosmological distance indicators. SNII are fainter, have a wider range in peak luminosity, and until recently were not as well studied.

The Supernova Legacy Survey (SNLS) carried out over 5 years from 2003 to 2008 with the CFHT has determined the rates of core-collapse and SNIa SN. Their cadence is such that there are at least 4 observations per lunation in each of their fields.

Preliminary results from the SNLS based on the first three years of data are given in the following papers. Bazin, Palanque-Delabrouille, Rich et al (2009, A&A, 499, 653) describe in detail the derivation of the SNII rate from their sample of 117 SNII confirmed by spectroscopy and/or detailed light curves. They find their rate to be larger than the SNIa rate by a factor of about 4.5, corresponding to $R(SNII) = 1.42 \times 10^{-4}$/yr/Mpc^3 at $z \sim 0.3$ for a Hubble constant of 70 km/sec/Mpc. The rate is proportional to $(H_0/70)^3$ if a different value for the Hubble constant is chosen.

Sullivan, Le Borgne, Pritchet et al (2006, ApJ, 648, 868) focus on the SNIa rate from the SNLS with a sample of 100 spectroscopically confirmed SNIa, plus 24 probable SNIa. They find a bivariate linear dependence with the SNIa rate per unit mass in a galaxy linearly proportional to the specific SFR (SFR/M_{gal}), i.e. to both the SFR and the stellar mass of the host galaxy, with $R(SNIa) = 5.3 \pm 1.1 \times 10^{-14}$ SN/yr/$M_\odot$ of the host galaxy and $3.9 \pm 0.7 \times 10^{-4}$/yr/SFR, where the SFR is in $M_\odot$/yr. This is equivalent to a prompt and a more delayed set of SNIa events from a burst of star formation.

Neill, Sullivan, Balam et al (2006, AJ, 132, 1126) use the SNLS to establishe the SNIa rate for a higher mean redshift ($z \sim 0.5$), but smaller sample of events.

Boticella, Riello, Cappellaro et al (2008, A&A, 479, 49) have published rates of SN at

intermediate redshift from the Southern Intermediate Redshift ESO SN Search (STRESS), but the number of spectroscopically confirmed SN is far below that of the SNLS, as is also the case for all previous surveys.

Moaz & Badenes (2010, MNRAS, in press, see arXiv:1003.3031) determine the SN rate and delay times in the Magellanic Clouds. Obviously they did not do this by counting SN, as 1987A is all we know about for sure. But there are 77 supernova remnants in the LMC and SMC, which they attempt to age date and separate into SNII and SNIa. A valiant attempt !

Nova rates are high enough that one can get a reasonable number of events per year detected in the Milky Way, about 4 per year (see the IAU telegrams, circulars, etc). Extrapolating that over the fraction not detected due to extremely high absorption, nd the area of the disk not searched, Della Velle & Livio (1994, A&A, 286, 786) estimate a rate of $\sim$20 novae per year. Della Valle, Rosino, Bianchini & Livio (1994, A&A, 287, 403) present preliminary results from a survey of novae in M33.

There have been a number of surveys of novae in M31, beginning with the classic work of H.C.Arp at Mount Wilson (1956, AJ, 61, 15). The PTF is conducting a survey of novae in nearby galaxies, including M31, M81, and several other galaxies. Darnley, Black, Bode et al (2009, arXiv:0809.4590) summarize in a conference proceedings their search for extragalactic classical novae in the Local Group, especially in M31.

Until very recently there were **no** detections of events that were claimed to be PISN. These are suggested to arise from a star with initial mass in excess of $140 M_{\odot}$, to produce very high energy explosions, during which the star becomes completely unbound and disrupts completely, without leaving a black-hole remnant. Such events may have been more common in the early Universe.

Very recently, SN2007bi was claimed by Gal-Yam, Mazzali, Ofek et al (2009, Nature, 462, 624) to be such an event. It was observed in a dwarf galaxy with $\sim$1% the mass of the Milky Way. They claim that the exploding core mass was about $100M_{\odot}$, and that more than $3M_{\odot}$ of ^{56}Ni was synthesized. This suggests that star-forming dwarf galaxies may host extremely massive stars, above the apparent limit for the Milky Way.

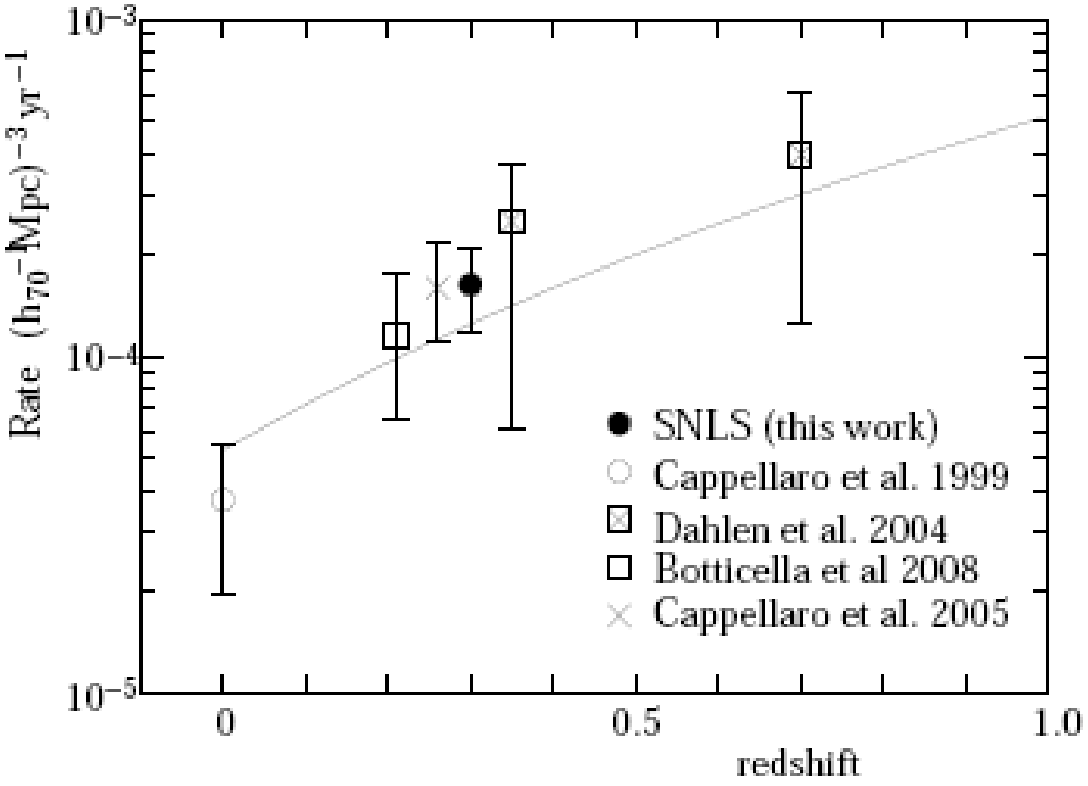

Fig. 13. The measured rate of SNcc as a function of redshift. The SNLS point includes a 15% correction for host absorption as described in the text. The error bars correspond to statistical and systematic uncertainties added in quadrature. The line is the best fit for rate$\propto (1+z)^{3.6}$, i.e. proportional to the SFR.

Fig. 13.— Fig. 13 of Bazin, Palanque-Delabrouille, Rich et al (2009, A&A, 499, 653)

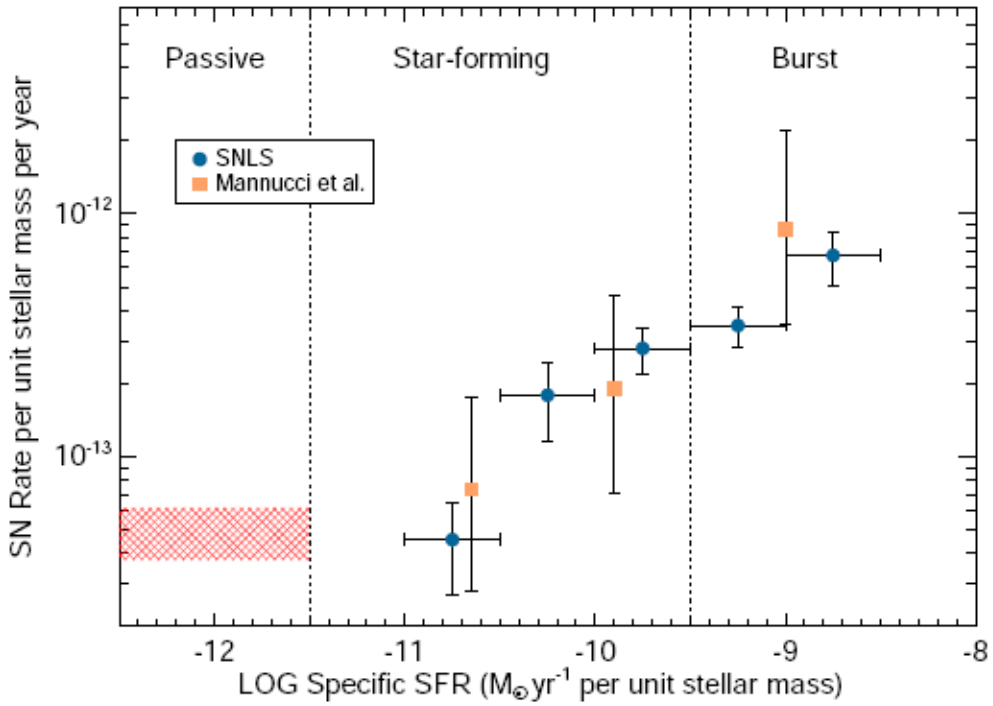

FIG. 6.— The number of SNe Ia per unit stellar mass as a function of the star-formation rate (SFR) per unit stellar mass of the host galaxy. Blue points represent SNLS data-points in star-forming galaxies. The red hashed area shows the number per unit stellar mass as measured in the SNLS passive galaxies (assigned zero SFR in our models). Shown for comparison is the evolution in SN Ia rate to later-type galaxies observed locally by Mannucci et al. (2005), normalized to the SNLS rate in passive galaxies. The horizontal positioning of the Mannucci et al. data points are subject to a uncertainty when converting their galaxy types into specific SFRs. The vertical dotted lines show the division we use to classify the host galaxies into different types.

Fig. 14.— Fig. 6 of Sullivan et al (2006).

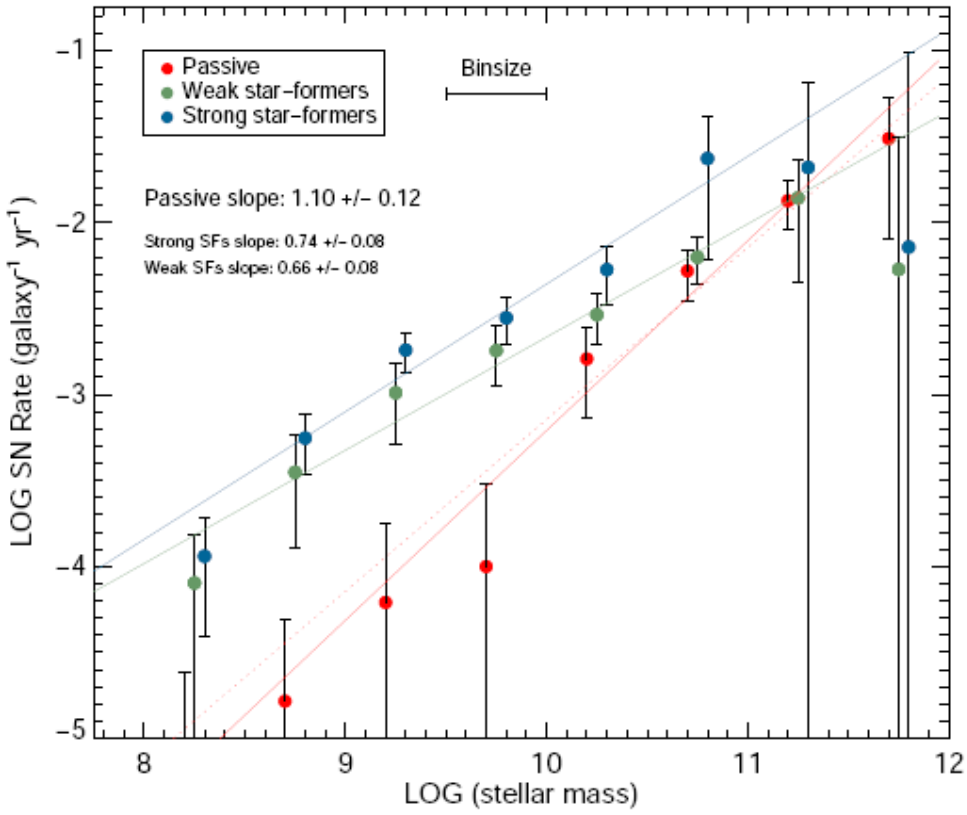

FIG. 8.— The number of SNe Ia per host galaxy as a function of host galaxy stellar mass. The three colors denote SNe Ia in the three different types of host galaxy as partitioned by their specific star-formation rate. The best-fitting lines and slopes to each distribution are shown. For the passive hosts, a line of slope unity is also shown (dotted line).

Fig. 15.— Fig. 8 of Sullivan et al (2006).

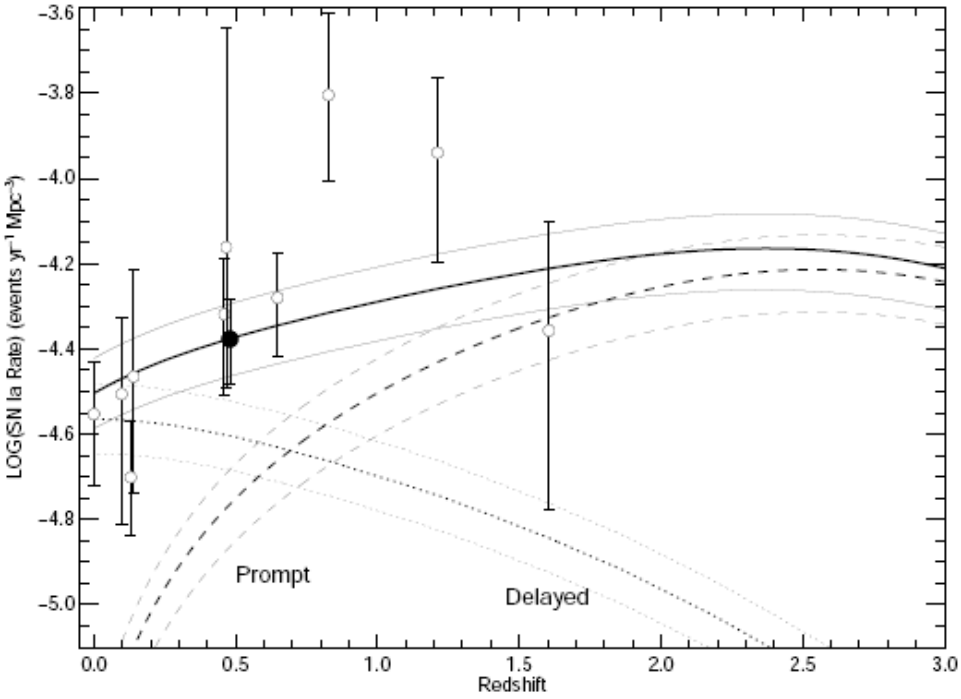

FIG. 10.— The predicted volumetric SN Ia rate as a function of redshift based on the A and B values from the bivariate fit of § 5.3. The dotted lines denotes the A "old" component (plus limits from the statistical errors), and the dashed line the B "prompt" component. The solid line shows the sum of the two. The filled circle is the $z = 0.47$ SNLS determination of the SN Ia rate of Neill et al. (2006). Open circles represent other SN Ia rate determinations from Cappellaro et al. (1999), Hardin et al. (2000), Pain et al. (2002), Tonry et al. (2003), Dahlen et al. (2004) and Blanc et al. (2004). We conservatively show the statistical and systematic error-bars added in quadrature where both are given in these papers. The star-formation history of Hopkins & Beacom (2006) is assumed.

Fig. 16.— The predicted SNIa rate as a function of redshift from their model, including both prompt and delayed contributions. The points are from analysis of images from various observational studies with suitable temperal cadence. The Palomar Transient Survey will be generate a much larger sample of SNIa, and hopefully improve the measurements of their frequency of occurent. The vertical axis is the number of SNIa events/yr/Mpc^3. Fig. 10 of Sullivan et al (2006).

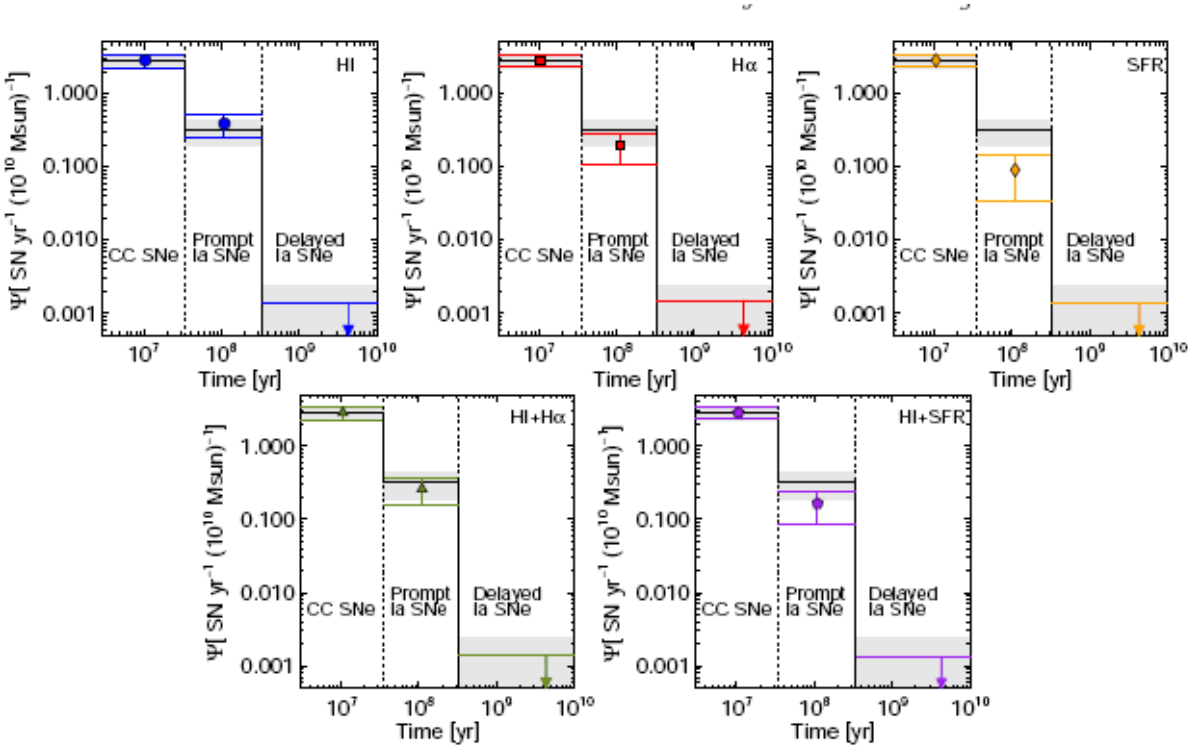

Figure 1. Best-fit delay-time distributions for the Magellanic Cloud SNR sample. Each panel in the top row displays the results obtained with a different density tracer: HI (left), Hα (centre), and SFR (right). The panels in the bottom row show the DTDs obtained with "hybrid" density tracers, using HI at low densities and either Hα (left) or SFR (right) at high densities. Error bars show 68% confidence intervals, from Monte-Carlo simulations that account both for Poisson statistics and for the uncertainties in the SFR of each cell. The best fits in the most-delayed bins are always zero, and the horizontal line gives the 95% confidence upper limit on the rate in this time bin. To facilitate comparison, the DTD obtained without scaling with density of the visibility time of SNRs is plotted in all panels as black lines, with shaded regions for the error bars. All DTDs have been scaled so as to give the same, theoretically expected, CC-SN yield in the first bin.

Fig. 17.— Fig. 1 of Maoz & Badenes (2010). SN rates in the LMC+SMC based on approximate age dating of SN remnants.

4. Other Types of Models

The numerical integration of models for chemical evolution of stellar populations described above has many parameters. One criticism is that there are enough "knobs" that almost any reasonable dataset can be reproduced, and that nothing is learned by applying such models.

Qian and Wasserburg have written a series of papers developing a phenomenological model. They specialize to simple cases, where the number of contributing types of sources is small. They adopt a fixed template of yield for each type of source, ignoring the complexities of differences of yield with progenitor mass. They look for specific element ratios which are diagnostic of which source contributes, and then compare that with the data. This simplification gives more insight into how good the template yields and list of specific types of sources might be, without getting lost in the many parameters that go into a full blown chemical evolution computation. Clearly this will work best when the number of types of sources is small. Thus they focus on the first few generations of normal stars in the Galaxy, before SNIa got going, and especially on the ratio of the heavy neutron capture elements vs Fe vs α-elements.

Their current model contains 3 sources, low mass SNII, normal mass SNII (both of which leave behind neutron stars and within which the r-process can operate) and and hypernovae (very energetic SNII), which leave a black hole. No heavy neutron capture occurs for hypernovae, which produce only elements through the Fe-peak, but not heavier. They claim that HNe produced 24% of the Fe in the Sun, while normal SNII contributed only 9% instead of the 33% normally assumed. They attribute the elements Sr through Ag, the first peak of heavy neutron capture elements) to charged particle reactions in neutrino driven winds from young neutron stars instead of the neutron capture, while the elements in the Ba peak and beyond they consider the true r-process elements produced by extensive

rapid neutron capture in low mass SN.

Key papers of theirs to read are: Qian & Wasserburg (2008, ApJ, 687, 272 and 2007, Physics Reports, 442, 237).

Of course, once there are many sources operating and many generations of stars contributing to the chemical inventory of the iSM, the situation rapidly becomes too complicated for such an approach, and a full numerical integration of the equations of chemical evolution is required.

Table 4. Characteristics of HNe, H, and L^* Sources

Sources	HNe	H	L^*
stellar types	HNe from stars of ~ 25–$50\,M_\odot$	low-mass SNe from stars of ~ 8–$11\,M_\odot$	normal SNe from stars of ~ 12–$25\,M_\odot$
remnants	black holes	neutron stars	neutron stars
nucleosynthetic characteristics	dominant source for low-A elements from Na through Zn $f^\odot_{\rm Fe,HN} \sim 0.24$[a]	source for CPR elements from Sr through Ag and only source for heavy r-elements with $A > 130$	source for low-A and CPR elements $f^\odot_{{\rm Fe},L^*} \sim 0.09$[b]

[a]Fraction of the solar Fe abundance contributed by HNe.

[b]Fraction of the solar Fe abundance contributed by the L^* source.

Fig. 18.— The three sources considered in the latest models of Qian and Wasserburg and the range of elements each is assumed to produce. (Table 4 of Qian & Wasserburg, 2008.)

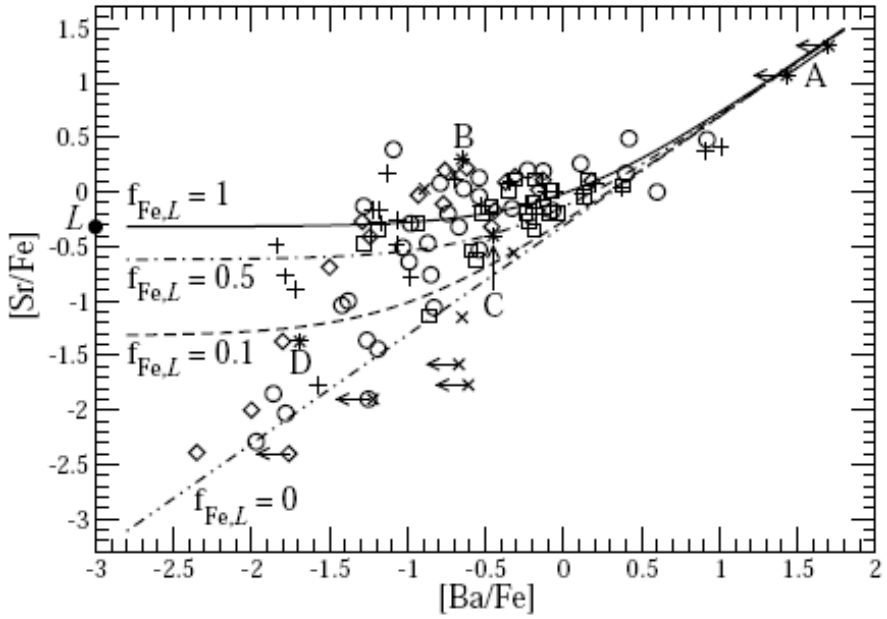

Fig. 2.— Evolution of [Sr/Fe] with [Ba/Fe]. Data symbols are the same as in Figure 1 except that the left-pointing arrows indicate the upper limits on [Ba/Fe]. Typical observational errors in [Sr/Fe] and [Ba/Fe] are $\sim$ 0.1–0.25 dex. The curves show $[\mathrm{Sr/Fe}] = \log\left(10^{[\mathrm{Sr/Ba}]_H + [\mathrm{Ba/Fe}]} + f_{\mathrm{Fe},L} \times 10^{[\mathrm{Sr/Fe}]_L}\right)$ based on the three-component model with the H and L sources and a third source (HNe) for $f_{\mathrm{Fe},L} = 0$ (dot-dot-dashed), 0.1 (dashed), 0.5 (dot-dashed), and 1 (solid). The parameter $f_{\mathrm{Fe},L}$ is the fraction of Fe contributed by the L source ($f_{\mathrm{Fe},L} = 0$ corresponds to all the Fe being from the third source). The filled circle labeled "L" indicates the value of $[\mathrm{Sr/Fe}]_L = -0.32$ for the L source. Almost all of the data lie within the allowed region of the model. Note the presence of quite a few data on the curve for $f_{\mathrm{Fe},L} = 0$ as well as the abundant data near the curve for $f_{\mathrm{Fe},L} = 1$.

Fig. 19.— Constraints on allowed ratios of [Sr/Fe] vs [Ba/Fe] from the models of Qian and Wasserburg. (Fig. 2 of Qian & Wasserburg, 2008.)

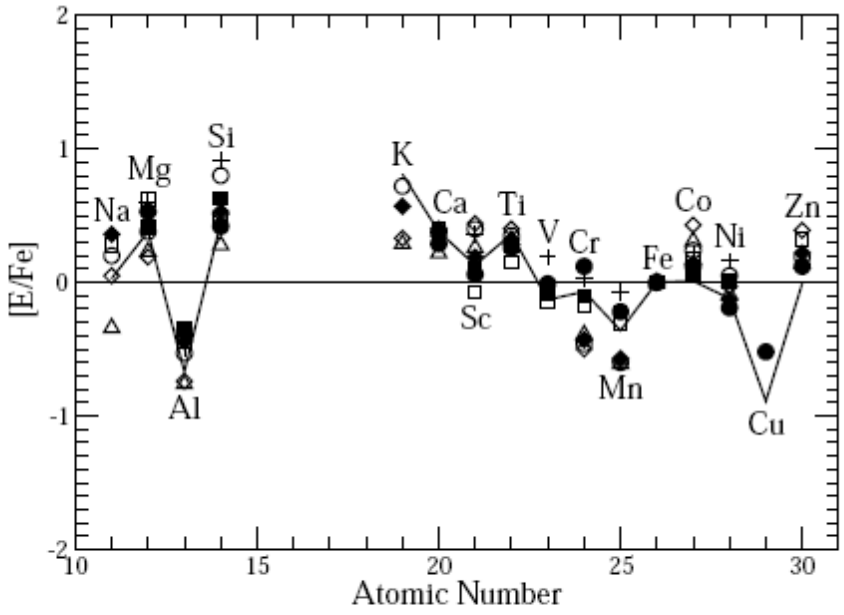

Fig. 6.— Comparison of the abundance patterns of the low-A elements for the third source (HNe) and the L source. The patterns for the third source are taken from five stars that lie on the curve for $f_{\mathrm{Fe},L} = 0$ in Figure 2 (open square: BD $-18°5550$, [Fe/H] $= -2.98$, Johnson 2002; open circle: CS 30325–094, [Fe/H] $= -3.25$, open diamond: CS 22885–096, [Fe/H] $= -3.73$, open triangle: CS 29502–042, [Fe/H] $= -3.14$, Cayrel et al. 2004; plus: BS 16085–050, [Fe/H] $= -2.85$, Honda et al. 2004). Those for the L source are from three stars that lie on the curve for $f_{\mathrm{Fe},L} = 1$ in Figure 2 (filled square: BD $+4°2621$, Johnson 2002; filled circle: HD 122563, Honda et al. 2004, 2006; filled diamond: CS 29491–053, Cayrel et al. 2004). The solid curve represents a star (BD $+17°3248$, Cowan et al. 2002) with a relatively high value of [Fe/H] $= -2$. Typical observational errors in [E/Fe] are ~ 0.1–0.25 dex. All the patterns shown are essentially indistinguishable.

Fig. 20.— Adopted template yields for the light elements through the Fe-peak for two of the three sources adopted by Qian & Wasserburg. The adopted production yields for these elements are assumed to be identical for hypernovae and for normal SNII. (Fig. 6 of Qian & Wasserburg, 2008.)

5. Topics For Discussion

1. Derive the solutions given above for $S(Z)$ and for X_S (the abundance of a secondary element) (eqs. 4 and 5) for the Simple Model with instantaneous recycling.

2. Look into the details of predicting the SNIa rate by reading papers by Laura Greggio and others.

2. Look into the details of calculating the SNIa and SNII rates from the SNLS observations by reading the papers cited above.